

# JGR Space Physics

## RESEARCH ARTICLE

10.1029/2021JA029812

### Key Points:

- The meteor height distribution was simulated using a meteor ablation model
- Simulation results show clearly the linear relationship between full widths at half maximum of the meteor height distribution and mesospheric temperatures
- Initial mass distributions of sporadic meteors derived from the King Sejong Station meteor radar are almost invariable over a year

### Correspondence to:

Y. H. Kim,  
[yhkim@cnu.ac.kr](mailto:yhkim@cnu.ac.kr)

### Citation:

Lee, W., Lee, C., Kim, J.-H., Kam, H., & Kim, Y. H. (2022). A modeling analysis of the apparent linear relation between mesospheric temperatures and meteor height distributions measured by a meteor radar. *Journal of Geophysical Research: Space Physics*, 127, e2021JA029812. <https://doi.org/10.1029/2021JA029812>

Received 19 JUL 2021  
Accepted 18 DEC 2021

### Author Contributions:

**Conceptualization:** Changsup Lee, Yong Ha Kim  
**Data curation:** Wonseok Lee, Changsup Lee, Jeong-Han Kim, Hosik Kam  
**Formal analysis:** Wonseok Lee  
**Funding acquisition:** Yong Ha Kim  
**Investigation:** Wonseok Lee  
**Methodology:** Wonseok Lee, Yong Ha Kim  
**Project Administration:** Yong Ha Kim  
**Resources:** Jeong-Han Kim, Yong Ha Kim  
**Software:** Wonseok Lee  
**Supervision:** Yong Ha Kim  
**Validation:** Hosik Kam, Yong Ha Kim  
**Writing – original draft:** Wonseok Lee  
**Writing – review & editing:** Changsup Lee, Jeong-Han Kim, Hosik Kam, Yong Ha Kim

## A Modeling Analysis of the Apparent Linear Relation Between Mesospheric Temperatures and Meteor Height Distributions Measured by a Meteor Radar

Wonseok Lee<sup>1</sup> , Changsup Lee<sup>2</sup> , Jeong-Han Kim<sup>2</sup> , Hosik Kam<sup>3</sup> , and Yong Ha Kim<sup>1</sup> 

<sup>1</sup>Department of Astronomy, Space Science, and Geology, Chungnam National University, Daejeon, South Korea, <sup>2</sup>Division of Atmospheric Sciences, Korea Polar Research Institute, Incheon, South Korea, <sup>3</sup>Space Science Division, Korea Astronomy and Space Science Institute, Daejeon, South Korea

**Abstract** A new method of estimating mesospheric temperature has recently been proposed by utilizing an apparent linear relation between atmospheric temperatures and full widths at half maximum (FWHMs) of meteor height distributions measured by a meteor radar (MR). However, the new method assumes that the meteor height distribution is dominantly dependent on the atmospheric conditions, rather than on meteoroid characteristics (mass and velocity). In order to verify this assumption, we have developed a meteor ablation model and applied it to the observed parameters by a MR at King Sejong Station (62.2°S, 58.8°W). The simulation results show that the FWHM of meteor height distribution increases linearly with the mesospheric temperature and its linear relation matches well with the observed relation. We found that the seasonal variation of meteor velocity distributions is significant but has only little effect on the variation of the height distribution. We also found that the observed characteristics of meteors are consistent with a Gaussian distribution of logarithmic masses, and this distribution is nearly invariable throughout the year with the average peak value of  $10^{-6.2}$  kg. Thus, we conclude that observed meteor height distributions are mainly dependent on the mesospheric temperature, and can be used as a mesospheric temperature indicator.

**Plain Language Summary** We have simulated meteor ablation to analyze the data observed by a meteor radar at an Antarctic station (King Sejong Station, 62.2°S, 58.8°W). We found that the simulated distribution of meteor heights are strongly dependent on the mesospheric temperature, rather than incoming meteor characteristics. The simulation confirms that mesospheric temperature can be estimated from the full width half maximum (FWHM) of the observed height distribution by the meteor radar, which was proposed by our previous work (C. Lee et al., 2016, <https://doi.org/10.1002/2016GL071082>).

## 1. Introduction

A few hundred tons of cosmic dusts and meteoroids come into the Earth's atmosphere a day (Murad & Williams, 2002). When a meteoroid penetrates into the atmosphere, its surface is heated up by collision between the meteoroid and the neutral atmosphere. Given its high entry velocity, the surface temperature of an incoming meteoroid reaches the boiling point and the surface is ablated. In the ablation process, the surface temperature is increased to  $\sim 1850$  K, producing a cylindrical plasma trail, called a meteor trail (Baggaley, 2002). A low power VHF meteor radar (MR) can detect the meteor trail in the mesosphere and lower thermosphere (MLT) day and night under almost all weather conditions. The MR can measure decay times, Doppler velocities, meteor velocities, and heights of meteors (Elford, 2004; Holdsworth et al., 2004). Using these observed parameters of meteors, the MR can provide not only the vertical profile of a neutral wind (e.g., W. Lee et al., 2021) but the daily mesospheric temperature continuously (e.g., Hocking, 1999; C. Lee et al., 2016). Although high power large aperture (HPLA) radars can detect head echoes of meteors in nonspecular directions, providing more information on various processes in the meteor plasma than the MR, the current study addresses only data from the low power MR. Data from HPLA radars have been analyzed by other groups of researchers, in terms of diffusion, turbulence, scattering that may occur in nonspecular trails (Close et al., 2008; L. Dyrud et al., 2008; L. P. Dyrud et al., 2005; Marshall & Close, 2015; Yee & Close, 2013; Zhou et al., 2004).

Traditionally, the diffusion coefficient profiles derived from the MR are used to estimate the mesospheric temperatures. In this temperature estimation, one has to adopt either a pressure model or a temperature gradient model for the background atmosphere. The pressure model method is based on the fact that the ambipolar diffusion

coefficient measured from a meteor trail is related to the atmospheric temperature and pressure (Cervera & Reid, 2000; Chilson et al., 1996; Hocking et al., 1997). Therefore, the pressure model method can in principle estimate a temperature profile from a measured diffusion coefficient profile, by utilizing a pressure model or local climatological pressure profiles. However, most of the studies have limited the pressure model method to the meteor peak height (MPH), where the maximum meteor count is detected, to guarantee the accuracy (M. E. Dyrlund et al., 2010; Hall et al., 2012; Holdsworth et al., 2006; Lima et al., 2018; Meek et al., 2013). The temperature gradient method, proposed by Hocking (1999), utilizes the slope of the scatter plot of logarithmic diffusion coefficient versus height and the temperature gradient at the MPH. Numerous studies using the temperature gradient method reported that their estimated temperatures are reasonably comparable to other ground-based measurements, satellite measurements, and empirical model (Holdsworth et al., 2006; Kam et al., 2019; Kim et al., 2012; Lima et al., 2018; Meek et al., 2013; Singer et al., 2004; Stober et al., 2008; Vineeth et al., 2005; Yi et al., 2016). However, there are some shortcomings in both methods. First of all, those methods have to use either a precise pressure or temperature gradient at the MPH from a model, and thus the results are model dependent. Second, the temperature gradient method requires the slope of the diffusion coefficient profile in the region where the ambipolar diffusion should be dominant. However, the altitude range for the dominant ambipolar diffusion varies with season and latitude (Kim et al., 2010; C. S. Lee et al., 2013; Premkumar et al., 2019), leading to the uncertainty in temperature estimation.

To overcome these shortcomings, C. Lee et al. (2016) suggested a new method to estimate mesospheric temperature based on the meteor height distribution without any additional information. They showed that the full width at half maximum (FWHM) of a meteor height distribution corresponds to the two constant pressure levels measured from the Microwave Limb Sounder (MLS) on board the Aura satellite. This means that the FWHM is immediately proportional to the mean temperature of the layer between the two pressure levels, based on the hypsometric equation. C. Lee et al. (2016) reported that the average difference of the FWHM method temperatures from the MLS temperatures is smaller than that of the temperature gradient method (using the slope of the diffusion coefficient profile) from the MLS temperatures, and its day-to-day variability is smaller, too. C. Lee et al. (2018) verified that the proportional constant between the FWHM of meteor height distribution and the temperatures from SABER is nearly invariable over 2012–2016. Kam et al. (2019) improved the temperature gradient method by applying strict criteria in selection of meteor echoes, but found that the temperatures from the FWHM method still shows better agreement with the MLS temperatures than those from the temperature gradient method. Based on these studies, one can suggest that the FWHM method is a better method for estimating the mesospheric temperature from an MR.

However, the FWHM method assumes that the meteor height distribution is dominantly dependent on the atmospheric condition, rather than on meteoroid characteristics (mass or velocity). According to Kaiser (1954), both the atmospheric pressure gradient and the meteoroid mass distribution can affect the width of meteor height distribution. Eshleman (1957) indicated that the length of a meteor trail is affected by the effects of meteoroid velocity, mass, entry angle, and the atmospheric scale height. In addition, Lindblad (1976) and Ellyett and Kennell (1980) suggested that the variations of the density gradient of neutral atmosphere control meteor detections. More recently, Younger (2011) found an approximate linear relationship between the width of the meteor height distribution and density scale height from numerical simulations. If the characteristics of meteoroids vary significantly with season, then the premise of the FWHM method would be weakened. Therefore, it is necessary to check whether the atmospheric condition can dominantly change the meteor height distribution, and whether the meteoroid mass distribution observed by an MR is invariant over the year to validate the FWHM method.

In this paper, we carried out a simulation of meteor ablation to verify the assumption of the FWHM method by using data from the King Sejong Station (KSS; 62.2°S, 58.8°W) MR and the NRLMSISE-00 model (Picone et al., 2002) over a full year period of 2017. From the simulation, we derived the relation between the mesospheric temperatures and the FWHM of the observed meteor height distribution. By tracing back the ablation process, we also computed the mass distribution of incoming meteoroids from observed parameters by the MR over the year.

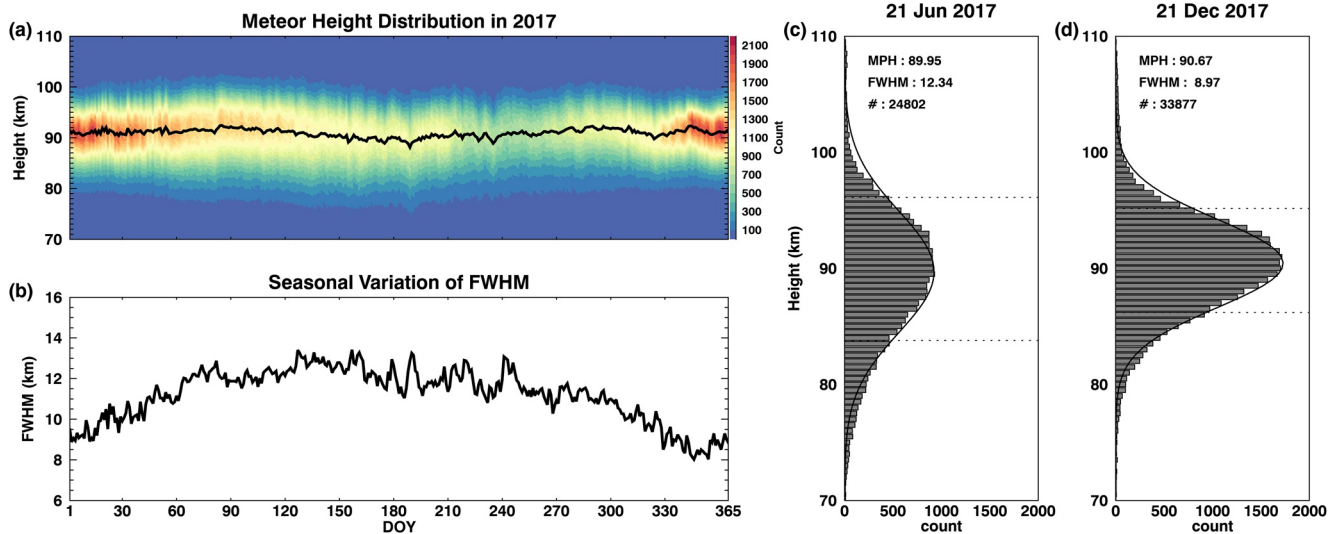


**Figure 1.** (a) Daily meteor height distributions in 2017, with a meteor peak height marked with a black line. The red color indicates high counts of meteor echoes. (b) Seasonal variation of the full width of half maximum (FWHM). (c) Meteor height distribution with a Gaussian fitting line in 21 June 2017, (d) same as (c) but in 21 December. The horizontal dotted lines indicate the FWHM.

## 2. Data

### 2.1. KSS Meteor Radar

The all-sky interferometric MR was installed in March 2007 at KSS and has been operating continuously. The frequency of the KSS MR is 33.2 MHz and its peak power is 12 kW since the MR was upgraded in 2012. The transmitter of KSS MR has the duty cycle of 8.4% for coded Gaussian shape pulse with a pulse repetition frequency of 440 Hz, and the maximum observable range is about 300 km. The detailed operating parameters of KSS MR are described in Kim et al. (2010). By upgrading the transmitter power to 12 kW in 2012, the KSS MR can detect about 15,000 ~ 40,000 underdense echoes a day with a seasonal variation, as shown in Figure 1a. The maximum count is observed in Southern Hemispheric (SH) summer and the minimum count is recorded during SH spring, as shown in Figure 1a. The MPH and FWHM can be derived from the Gaussian fitting of the daily meteor height distribution, as indicated in Figures 1c and 1d. Note that the asymmetry of meteor height distributions compared to the Gaussian fitting curves is related to the effect that backscattered signals from meteor trails at higher altitudes are significantly attenuated (C. Lee et al., 2018). Figure 1 clearly demonstrates that the FWHM of the meteor height distribution is large in SH winter, from June to August, when the mesospheric temperature is relatively high (~220 K) and the FWHM is small in SH summer, when the temperature is low (~170 K).

### 2.2. Aura/MLS

The MLS is one of four instruments on board the NASA's Earth Observing System (EOS) Aura satellite. The Aura satellite was launched on 15 July 2004 and has been an important source of information on Earth's atmosphere, as well as Terra and Aqua which were launched at 1999 and 2002, respectively. The Aura satellite is in a sun-synchronous polar orbit with an orbital inclination of 98.2° at the altitude of 705 km. The period of orbit is approximately 100 min, which means that the satellite rotates the Earth about 14 times per a day. The MLS utilizes a microwave limb sounding to derive vertical profiles of chemical species, temperature, pressure, and geopotential height (GPH) from the troposphere to upper mesosphere. Among these parameters, we used the temperature profiles to derive the temperature at the MPH near KSS, namely within a radius  $\leq 500$  km from KSS. The geometric height is calculated by using the GPH from the EOS MLS version 4.2x level 2 data. From the data quality document ([https://mls.jpl.nasa.gov/data/v4-2\\_data\\_quality\\_document.pdf](https://mls.jpl.nasa.gov/data/v4-2_data_quality_document.pdf)), we selected the temperatures and GPH profiles from 261 to 0.001 hPa with the quality greater than 0.2 and convergence less than 1.03. Since the MLS provides the data about twice a day, we use the daily temperature by averaging the day and night data.

### 3. Simulation of Meteor Ablation

Three main equations constitute the simulation of meteor ablation, and they are related to a loss of meteoroid mass, momentum, and energy (Brown et al., 2017; Campbell-Brown & Koschny, 2004; Ceplecha et al., 1998). When a meteoroid enters into the Earth's atmosphere and reaches near the altitude of 120 km, the meteoroid starts to be ablated. In this process, electrons are produced in the meteor trail as seen by all-sky MRs, whose size is about kilometers in length and a few atmospheric mean free paths in width (Baggaley, 2002). The electron density generated in the trail is usually described with an electron line density, because the trail length is much longer than the width. The electron line density is proportional to the mass loss rate of meteoroid and the effective ionization coefficient, and the relation can be expressed as

$$\frac{dm}{dt} = -\frac{qm_a v}{\beta} \quad (1)$$

where  $m$  is the meteoroid mass,  $q$  is the electron line density,  $v$  is the meteoroid velocity,  $m_a$  is the mean mass of ablated atoms, and  $\beta$  is the effective ionization coefficient (Baggaley, 2002). We adopt  $8.3 \times 10^{-26}$  kg for  $m_a$  from McAuliffe and Christou (2006). Although meteoroids can fragment, the backscattered power received at the radar is determined by the electron line density within the Fresnel zones near the specular point that encompass most of the fragments (Stober et al., 2011). The effective ionization coefficient represents the ratio of the number of generated electrons to the evaporated atoms, which depends on the meteoroid velocity (Jones, 1997). Jones (1997) suggested that when the meteoroid velocity is slower than 35 km/s and there is no secondary ionization or recombination,  $\beta$  can be calculated with

$$\beta = 9.4 \times 10^{-6} (v - v_0)^2 v^{0.8} \quad (2)$$

where  $v_0$  is the threshold velocity of a meteoroid below which the ionization does not occur. The constant and threshold velocity can vary depending on the meteoroid constituent. We use 10 km/s for the threshold velocity (Jones, 1997). Jones (1997) also proposed that if a meteoroid has the velocity range between 30 and 60.5 km/s, the effective ionization coefficient can be expressed as

$$\beta = 4.91 \times 10^{-6} v^{2.25}. \quad (3)$$

Rogers et al. (2005) and Stober et al. (2011) indicated that two different physical processes produce the electrons within the meteor trail: thermal ablation and sputtering. In the simulation, we ignored the sputtering process because it occurs above the altitude of 120 km and only important on a small ( $\sim 10$   $\mu\text{m}$ ) and fast ( $\sim 70$  km/s) meteoroid (see McAuliffe & Christou, 2006 and references therein). Therefore, only thermal ablation process creates the electrons and it can be expressed as

$$\frac{dm}{dt} = -4Am^{2/3}\rho_m^{-2/3}P_v\sqrt{\frac{m_a}{2\pi k_B T_m}}, \quad (4)$$

where  $A$  is the meteoroid shape factor,  $\rho_m$  is the density of the meteoroid,  $P_v$  is the saturated vapor pressure in Pa unit,  $k_B$  is the Boltzmann constant, and  $T_m$  is the temperature of meteoroid surface. The temperature of the meteoroid surface rapidly increases as the meteoroid enters into the atmosphere. As a result, the surface temperature reaches the boiling temperature, evaporating the meteoroid. The evaporation will proceed until the saturated vapor pressure is reached. The saturated vapor pressure can be obtained by the Clausius-Clapeyron equation.

$$P_v = 10^{C_A - \frac{C_B}{T_m} + 1}, \quad (5)$$

where  $C_A$  and  $C_B$  are Clausius-Clapeyron coefficients which depend on constituents of a meteoroid. Assuming rocky meteoroids, we adopted  $C_A$  and  $C_B$  as 13.176 and 24605 K, respectively (McAuliffe & Christou, 2006).

The collisions with atmospheric constituents and the Earth's gravity decelerate and accelerate a meteoroid, respectively. Since the velocity of meteoroid has the order of tens of kilometers per second, the effect of Earth's gravity component is significantly small. According to Stober et al. (2011), the total force is given by

$$m \frac{dv}{dt} = -\frac{C_w A m^{2/3}}{\rho_m^{2/3}} \rho_{\text{air}} v^2 + G \frac{Mm}{(R+h)^2}, \quad (6)$$

**Table 1**  
*Values in the Meteor Ablation Model*

Symbol	Definition	Value	Reference
$\beta$	Effective ionization coefficient	-	Baggaley (2002)
$m$	Meteoroid mass	-	-
$q$	Electron line density	-	-
$v$	Meteoroid velocity	-	-
$m_a$	Mean mass of ablated atoms	$8.3 \times 10^{-26} \text{ kg}$	Hunten et al. (1980)
$v_0$	Threshold velocity	10 km/s	Jones (1997)
$C_w$	Drag coefficient	1.0	Campbell-Brown and Koschny (2004)
$A$	Meteoroid shape factor	1.21	McKinley (1961)
$G$	Gravity constant	$6.67 \times 10^{-11} \text{ Nm}^2 \text{ kg}^{-2}$	-
$\rho_m$	Meteoroid density	$3.4 \times 10^3 \text{ kg/m}^3$	Moses (1992)
$\rho_{air}$	Density of the atmosphere	-	From NRLMSISE-00
$M$	Mass of the earth	$5.97 \times 10^{24} \text{ kg}$	-
$R$	The earth's radius	6371.0 km	-
$h$	height of the meteor	-	-
$k_B$	Boltzmann constant	$1.38 \times 10^{-23} \text{ J/K}$	-
$T_m$	Meteoroid surface temperature	-	-
$T_{air}$	Temperature of the atmosphere	-	From NRLMSISE-00
$P_v$	Saturated vapor pressure	Pa unit	-
$C_A$	Clausius-Clapeyron coefficients	13.176	Podolak et al. (1988)
$C_B$	Clausius-Clapeyron coefficients	24605 K	Podolak et al. (1988)
$\Lambda$	Heat-transfer coefficient	1.0	McAuliffe and Christou (2006)
$\sigma$	Stefan Boltzmann's constant	$5.67 \times 10^{-8} \text{ Wm}^{-2} \text{ K}^{-4}$	-
$L$	Latent heat ( $T_m < 1800 \text{ K}$ )	$8.1 \times 10^6 \text{ J/kg}$	Moses (1992)
	Latent heat ( $T_m > 1800 \text{ K}$ )	$6.7 \times 10^6 \text{ J/kg}$	Moses (1992)
$\epsilon$	Thermal emissivity of meteoroid	1.0	Hunten et al. (1980)
$C$	Heat capacity of meteoroid	$9.6 \times 10^2 \text{ Jkg}^{-1} \text{ K}^{-1}$	Moses (1992)

where  $C_w$  is the drag coefficient,  $\rho_{air}$  is the density of neutral atmosphere, and  $G$  is the gravitational constant.  $M$  and  $R$  is the mass and radius of the earth, and  $h$  is the height of the meteor. We used the drag coefficient  $C_w = 1$  and the shape factor  $A = 1.21$  for the spherical shape of meteoroid as proposed by Campbell-Brown and Koschny (2004) and McKinley (1961), respectively.

A meteoroid can gain or lose its thermal energy by collision with the atmosphere, radiation, and evaporation of meteoroid constituents (McAuliffe & Christou, 2006; Stober et al., 2011). The change rate of the thermal energy can be expressed as

$$mC \frac{dT_m}{dt} = \frac{\Lambda \rho_{air} v^3}{2} A \left( \frac{m}{\rho_m} \right)^{\frac{2}{3}} - 4\epsilon \sigma (T_m^4 - T_{air}^4) A \left( \frac{m}{\rho_m} \right)^{\frac{2}{3}} - L \frac{dm}{dt}, \quad (7)$$

where  $C$  is the heat capacity of the meteoroid,  $T_m$  is the surface temperature of the meteoroid,  $\Lambda$  is the heat-transfer coefficient,  $\epsilon$  is the thermal emissivity of meteoroid,  $\sigma$  is the Stefan Boltzmann's constant, and  $L$  is the latent heat of evaporation. The  $A(m/\rho_m)^{2/3}$  is the effective area of the meteoroid (Campbell-Brown & Koschny, 2004). The left-hand side term represents the heat storage. On the right side, the first term is the energy from the collision between the meteoroid and the atmosphere. The second and third terms on the right-side represent the radiative energy and the energy from the evaporation of the meteoroid, respectively. All the parameters in Equations 1–7 and their values with references are listed in Table 1.

From Equations 1–7, one can estimate the meteoroid surface temperature, meteoroid mass, and the deceleration of the meteoroid as functions of altitude. Substituting Equations 4 and 5 into the energy balance equation (Equation 7) yields the transcendental equation for meteoroid surface temperature. In the ablation process, the heat capacity term can be ignored because the meteoroids are small and thus isothermal. According to Stober et al. (2011), the heat capacity term is relatively smaller than other terms by about one to three order of magnitude. In other words, the energy from the atmospheric collision can be instantaneously lost by the radiation and evaporation. The transcendental equation was solved to derive the meteoroid surface temperature by the numerical iteration with the accuracy of 1 K. Substituting the surface temperature of meteoroid can compute the meteoroid mass at the observed altitudes using Equation 1.

The electron line density used in Equation 1 can only be determined when the absolute power of the received signal for a meteor or the antenna gain is clearly known (McKinley, 1961), with a relation:

$$q = B\sqrt{\text{received power} \times \text{range}^3}. \quad (8)$$

When the received power and range (distance between the antenna and a meteor) are known with an appropriate calibration factor,  $B$ , Equation 8 computes the electron line density in the absolute unit. However, the KSS MR does not provide its antenna gain, thus unable to set the received power in the absolute unit. Thus, we estimated the electron line density from a received power for an echo signal in an arbitrary unit by adjusting the coefficient  $B$ . By adopting  $B = 60$ , we were able to match the range of the computed mass distribution to the mass range of  $10^{-10}$ – $10^{-5}$  kg, which was suggested to be the mass range of meteoroids detected by a MR (Murad & Williams, 2002). Ceplecha et al. (1998) mentioned that the mass range from radar meteoroids are  $3 \times 10^{-9}$ – $3 \times 10^{-6}$  kg, while Mathews et al. (2001) reported that the radar observations indicate the mass range of  $10^{-14}$ – $10^{-7}$  kg. Besides, by using  $B = 60$ , we were able to obtain the MPH of simulated meteor height distribution around 90 km. Note that the computed meteoroid mass is affected by a factor of  $B^{1.5}$ , according to Equations 1 and 4. Although our computed meteoroid mass can differ from the absolute mass scale by a calibration factor, the FWHM of logarithmic mass distribution, in principle, should not be affected by the uncertainty of the adopted coefficient,  $B$ , because all the meteoroid masses are scaled with the same factor.

In the process of obtaining the surface temperature and mass of a meteoroid from Equations 4 and 6, we computed backward  $dm/dt$  and  $dv/dt$  from the measured parameters with a time step of  $10^{-2}$ s until the ablation is no longer effective above the altitude of 120 km (entry height). We regarded the mass and velocity at the entry height as the initial mass and velocity.

In order to validate the ablation model, we carried out the simulation with different sets of initial conditions at the entry height. The simulation of the ablating processes computes masses, surface temperatures, and electron line densities along the path as an incoming meteoroid interacts with the atmosphere whose condition is adopted from the NRLMSISE-00 model on DOY 100 2017 (10 April 2017). For Figure 2a, the same entry angle ( $45^\circ$ ) and initial velocity (30 km/s) but with different initial masses, and for Figure 2b, the same initial mass of  $1.45 \times 10^{-6}$  kg and entry angle of  $45^\circ$  but with different initial velocities were used in the simulation. For Figure 2c, the simulation was executed with the same initial mass  $1.45 \times 10^{-6}$  kg and initial velocity 30 km/s, but with different entry angles. Figure 2 displays that the meteoroid mass is hardly changing at the first 10 km or so from the entry height, and then steeply decreasing as it penetrates deeper in the atmosphere. This behavior confirms that the starting altitude of 120 km can be regarded as the entry height. The height where the computed electron line density is maximized in the simulation can be assumed as the observed altitude of a meteor trail by the MR because the radar has the highest chance to detect a meteor echo at the maximum electron line density, which was suggested by Baggaley (2002). The results of simulations in Figure 2 indicate that a meteor would be observed by the MR at an altitude of 3.9 km lower and 1.6 km higher if its initial mass and velocity increase by 10 times and by 5 km/s, respectively. The meteor altitude would occur 1.2 km lower if the entry angle becomes  $15^\circ$  steeper.

In reality, the observed height would be determined by the minimum detectable line density, which may be either above or below the height of maximum line density (Ceplecha et al., 1998; McKinley, 1961). Since we do not have information on the minimum detectable line density for the KSS MR, we have to rely on the maximum line density height (Qmax height) as a measure of the predicted meteor height. We simulated Qmax heights for the DOY 100 echoes and compared with the observed heights, as shown in Figure 3. The mean difference between observed heights and the Qmax heights is  $\sim 0.8$  km for the DOY 100 echoes and the mean absolute difference

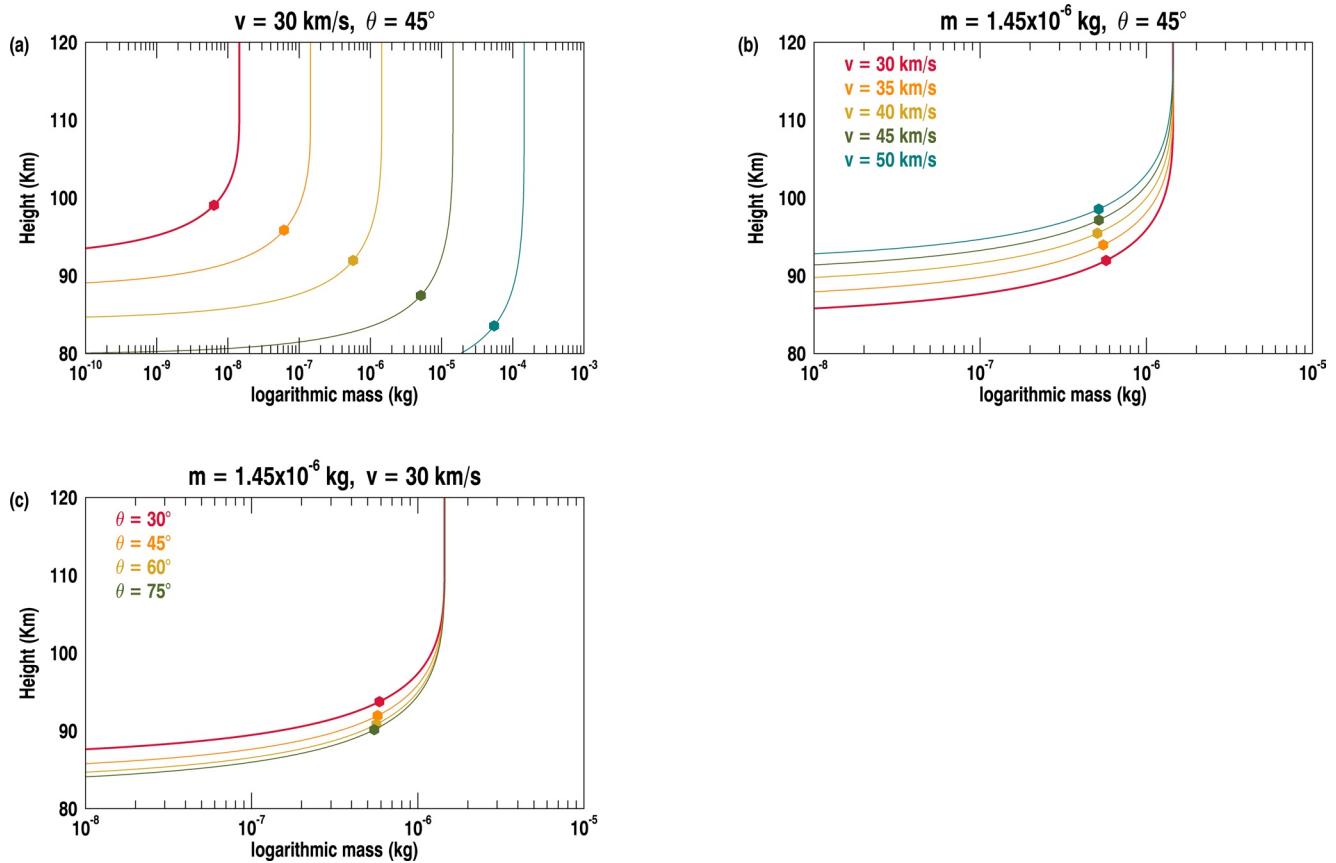


**Figure 2.** Simulation results for different sets of initial conditions. (a) initial velocity = 30 km/s and  $45^\circ$  entry angle, but different initial masses, (b) initial mass =  $1.45 \times 10^{-6} \text{ kg}$  and  $45^\circ$  entry angle, but different initial velocities, 30 ~ 50 km/s, and (c) initial mass =  $1.45 \times 10^{-6} \text{ kg}$  and initial velocity = 30 km/s, but different entry angles  $30^\circ \sim 75^\circ$ . The filled circles indicate the observed height where the electron line density is maximized.

is 3.9 km. The seemingly large scatter from the 1:1 line, fortunately, is canceled out when the FWHM of the simulated height distribution is computed. On this day, the simulated and observed FWHM are 12.2 and 11.6 km (Figure 3b), whose difference is so small that it doesn't spoil the FWHM relation to the mesospheric temperature in the simulation. In our simulation, if the range of meteoroid has a 7 km uncertainty at the  $45^\circ$  entry angle, the  $Q_{\text{max}}$  height is changed by  $\sim 0.5 \text{ km}$ . In addition, the 10% of error in angle of arrival ( $\sim 6^\circ$ ) makes the uncertainty of  $\sim 0.6 \text{ km}$  in the  $Q_{\text{max}}$  height. The uncertainties in range and angle of arrival might affect the FWHM of the simulated meteor height distribution as much, but the relationship between FWHM and mesospheric temperature can be still verified.

Applying the ablation model to the KSS MR data, we can derive the mass distribution of meteors at the observed height. By computing the model backward in time we were also able to obtain the mass distribution at the entry height of 120 km. In the calculation process, the hourly atmospheric conditions (density and temperature) were again adopted from the NRLMSISE-00 model. Note that the computed mass in both distributions is an estimated meteoroid mass, which may differ from an absolute mass by the calibration factor in the electron line density estimation, as explained above. The total number of observed echoes on this day was 35,668, but the number of echoes that were applied to the ablation model is 17,123. Since a single MR cannot provide the entry angle of meteor, we assume that the meteors observed at a specific azimuth angle passed through the zenith of the observation site, and these meteors are from the helion source which is located about  $70^\circ$  to the left of the Earth's motion (Taylor & Elford, 1998). Under this assumption, we can regard the zenith angle of observed echoes as the entry angle of the helion meteors that would appear with the specific azimuth angle at different local time. To make the entry angle assumption reasonable, we selected only the echoes within  $\pm 60^\circ$  in azimuth where the most echoes are observed at each time bin (1 h) because the helion source is the major contributor of meteors. Figure 4 shows the logarithmic distributions of the meteoroid masses at observed height (gray) and at the entry height (olive) on

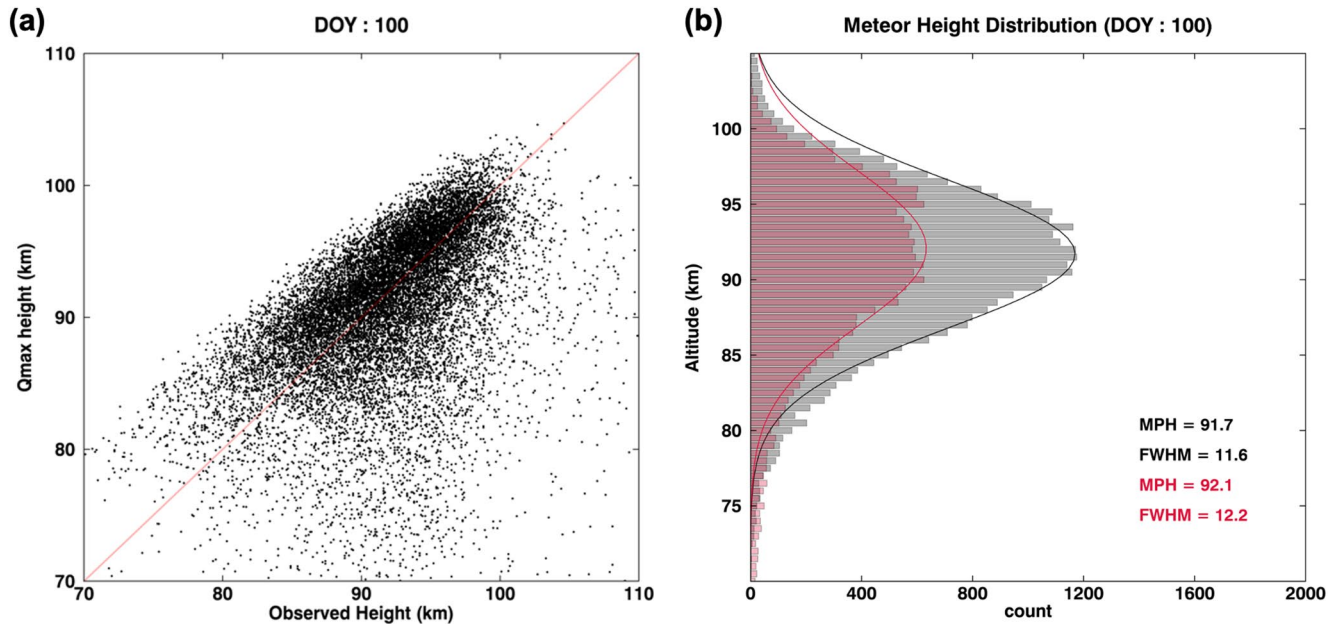


**Figure 3.** (a) The scatter plot of observed meteor heights versus simulated meteor heights (Qmax height: the height where the calculated electron line density is maximum) using the DOY 100 echoes. The red line indicates the 1:1 line. (b) Observed meteor height distribution (gray histogram) and simulated meteor height distribution (red histogram) on DOY 100, overlapped with Gaussian fitting lines.

10 April 2017. It is evident from Figure 4 that the median of initial (entry height) mass distribution ( $10^{-6.1}$  kg) is more massive by about 6.3 times than that of the observed mass distribution ( $10^{-6.9}$  kg).

In order to verify the method of estimating neutral temperature from the FWHM of meteor height distribution, we first simulate the meteor height distribution using the DOY 100 (10 April 2017) meteoroid group under the different atmospheric conditions. The simulation started with the initial mass distribution computed from the DOY 100 meteoroid group at the entry height, and went through the interaction with the atmosphere on two different days.

The height where each meteoroid sheds off the maximum mass in the simulation (thus maximum electron line density along the trail) is recorded to obtain the meteor height distribution that would be observed on the given day. We selected the two days which have the relatively high and low temperatures near the mesopause region and compared the simulated meteor height distributions. The left panel of Figure 5 illustrates the daily NRLMSISE-00 temperature profiles on DOY 123 (3 May; red line) and on DOY 7 (7 January; blue line) in 2017. The temperature at 91 km on DOY 123 is higher by about 52 K than that on DOY 7. In the right panel of Figure 5, both simulated meteor height distributions have the similar MPH ( $\sim 91$  km) but their FWHMs differ by about 3.6 km: the FWHM on DOY 123 (Temp. at 91 km is 201 K) is 12.3 km and that on DOY 7 is 8.7 km (Temp. at 91 km is 149 K). Therefore, the simulation verifies that the higher mesospheric temperature leads to the larger FWHM.

#### 4. Results and Discussion

Since the velocity distributions of sporadic meteors are known to change seasonally due to the viewing geometry of the site (Holdsworth et al., 2008; Younger et al., 2009), we selected two meteoroid groups in different seasons to investigate the effect of the velocity distribution on the meteor height distribution. Figure 6 shows the initial velocity and mass distributions that were computed from MR data measured on DOY 100 and DOY 200, respectively.

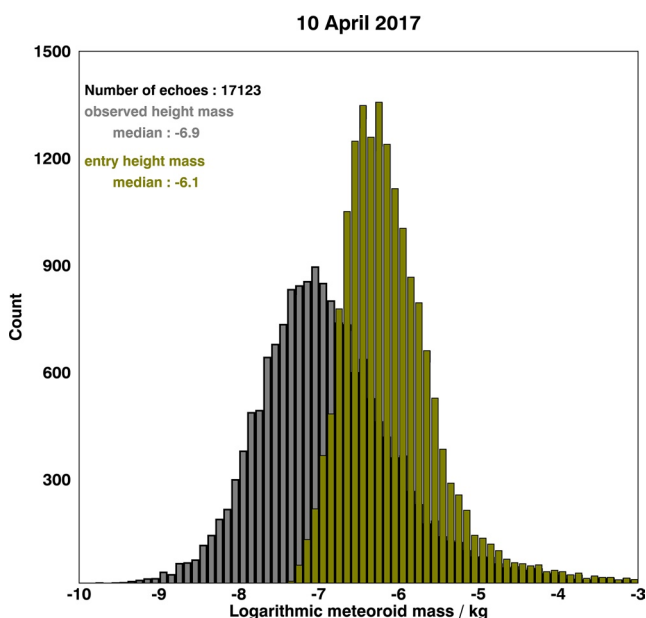


**Figure 4.** Mass distributions at the observed height (gray) and at the entry height (olive) on the 10 April 2017.

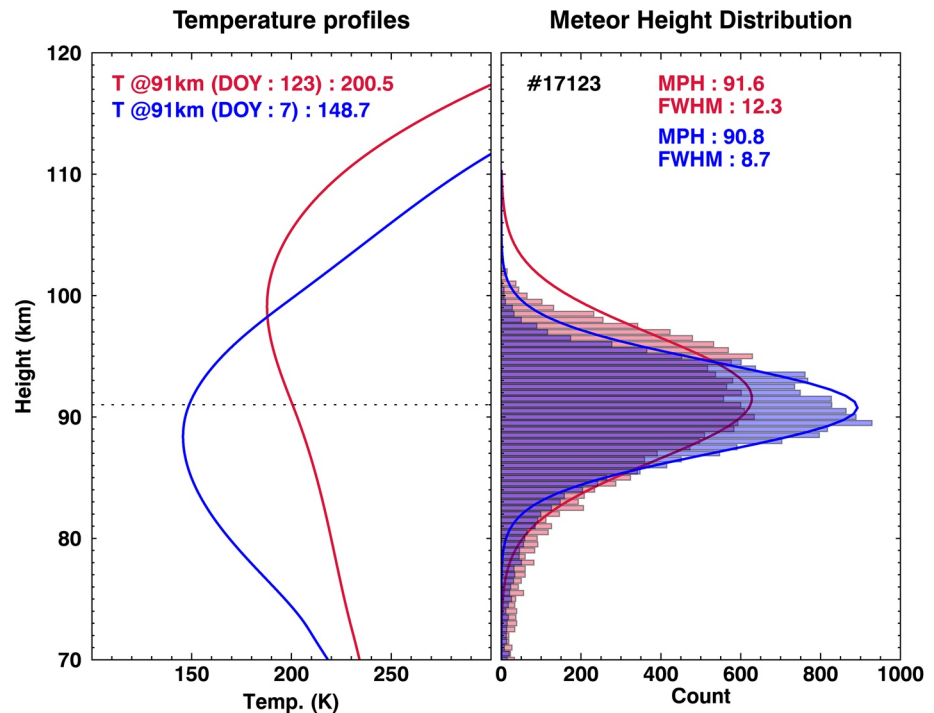


**Figure 5.** (Left) Daily NRLMSISE-00 temperature profiles on DOY 123 (red line) and 7 (blue line) in 2017. MPH (~91 km) is marked with a dotted line. (Right) Simulated meteor height distributions on DOY 123 (red histogram) and 7 (blue histogram) using the same distribution of meteors with Gaussian fitting lines.

The shapes of initial mass distributions for the days are almost identical, but there is a distinguishable difference in the initial velocity distributions. The meteoroid group for DOY 100 has double peaks near the 30 km/s and 50 km/s, whereas the DOY 200 group has a single peak near the 35 km/s. According to Campbell-Brown (2008), the high speed meteoroids come from the apex source, in the range of 45–70 km/s, while the meteoroids from the helion source have speeds of 20–35 km/s. Thus, both the helion and apex sources mainly constitute the meteoroid velocity distribution observed by MR on DOY 100 (Figure 6a), while the helion source dominates the meteors on DOY 200 (Figure 6b). In addition, the apparent spike around 35–40 km/s on DOY 200 (Figure 6b) might be the contribution of the Southern Delta Aquarids meteor shower, which contains the meteoroids with velocities around 40 km/s (McKinley, 1961).

Applying the initial velocity and mass distributions of the DOY 100/DOY 200 meteoroid groups to the ablation model, we calculated the meteor height distributions for 12 days (one day in each month; DOY 7, 38, 66, 100, 123, 162, 199, 230, 263, 288, 315, and 348). Those days are selected to cover the range of seasonal mesospheric temperature variation and the absolute difference of temperature at 90 km between MLS and NRLMSISE-00 is less than 10 K. Figure 7a shows the seasonal variations of temperatures at 90 km from MLS (black line) and NRLMSISE-00 (red line) in 2017, and their differences are presented in Figure 7b. In Figure 7, the selected days for the ablation modeling are indicated with gray shaded area. Note that the model temperatures do not differ significantly from MLS temperatures, implying that the model atmosphere used in the simulation reasonably represents the actual atmosphere.

Figure 8 displays the scatterplot of the daily FWHMs of meteor height distributions observed by KSS MR versus the MLS temperatures at 90 km (gray circles) as well as the scatterplot of the FWHMs of the simulated meteor height distributions using the meteoroid groups of DOY 100 and 200 versus NRLMSISE-00 temperatures at 90 km for 12 days (red and blue dots).

Both simulations for DOY 100 and 200 in Figure 8 clearly indicate that the FWHMs increase with atmospheric temperatures, which is consistent with the apparent linear relation between the observed daily FWHMs and the atmospheric temperatures. Notably, the DOY 100 simulation almost perfectly matches the observed linear relation (the slope: 16.64 and 16.69 for observation and the DOY 100 simulation, respectively), with the very small

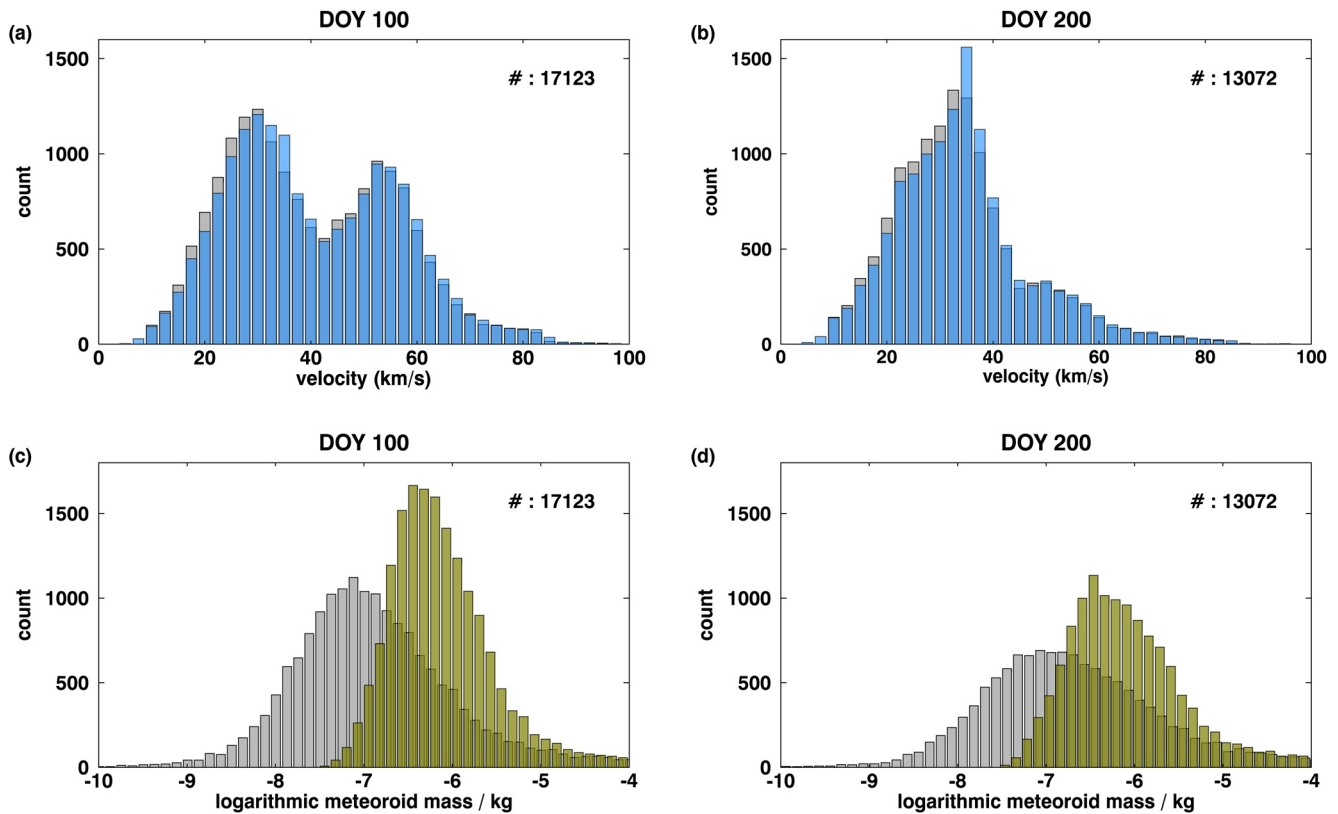


**Figure 6.** (a and b) Initial velocity distributions for DOY 100 and DOY 200, respectively. (c and d) Initial mass distributions for DOY 100 and DOY 200, respectively. The number of echoes is 17,123 and 13,072 for DOY 100 and DOY 200, respectively. For the comparison, distributions at observed heights are overlapped (gray).

mean difference of 0.11 km. Although the DOY 200 simulation differs significantly from the observed relation (the slope and mean difference: 20.75 and 2.5 km for the DOY 200 group), it still shows the linear relationship between the FWHM and atmospheric temperature.

According to Figure 6, the DOY 200 meteoroid group lacks high speed meteoroids ( $> \sim 40$  km/s). Considering that the high speed meteoroids ablate in the high altitude region as shown in Figure 2b, the lack of high speed meteoroids affects the meteor height distribution above the MPH, making the FWHM of the simulated height distribution smaller for a given atmospheric temperature. This characteristic implies that if the velocity distribution of incoming meteoroids varies with seasons adversely (less high speed meteoroids during warmer seasons), the observed positive relation between the FWHM and atmospheric temperature would have been ruined. Fortunately, the initial velocity distribution computed from the KSS MR data varies with season significantly but not adversely, as shown in Figure 9. Specifically, the high speed meteoroids are reduced in spring and early summer (September–early December) when the mesosphere is colder. Thus, our simulation confirms the observed positive relation, even if the velocity distribution of meteoroid changes with seasons. For other radar stations, the viewing geometry of the sources is different from the KSS MR so that the distributions of observed meteoroid velocity can be changed. It means that the linear relationship might be different from the KSS MR depending on the latitude of radar site. Further works are needed to figure out how a radar viewing geometry at different latitude affects the linear relationship between the FWHMs and mesospheric temperatures.

Since the simulated height distribution also depends on the initial mass distribution, in addition to the velocity distribution, it is necessary to check whether the meteoroid mass distribution varies significantly throughout the year. We calculated initial mass distributions from daily observed parameters by the MR in 2017. The calculated mass distributions are plotted daily with a normalized logarithmic contour format in Figure 10a, and their Gaussian peaks and FWHMs are displayed in Figures 10b and 10c. It is evident from Figure 10 that the mass distributions are nearly invariable throughout the year. The logarithmic distributions are nearly a Gaussian shape

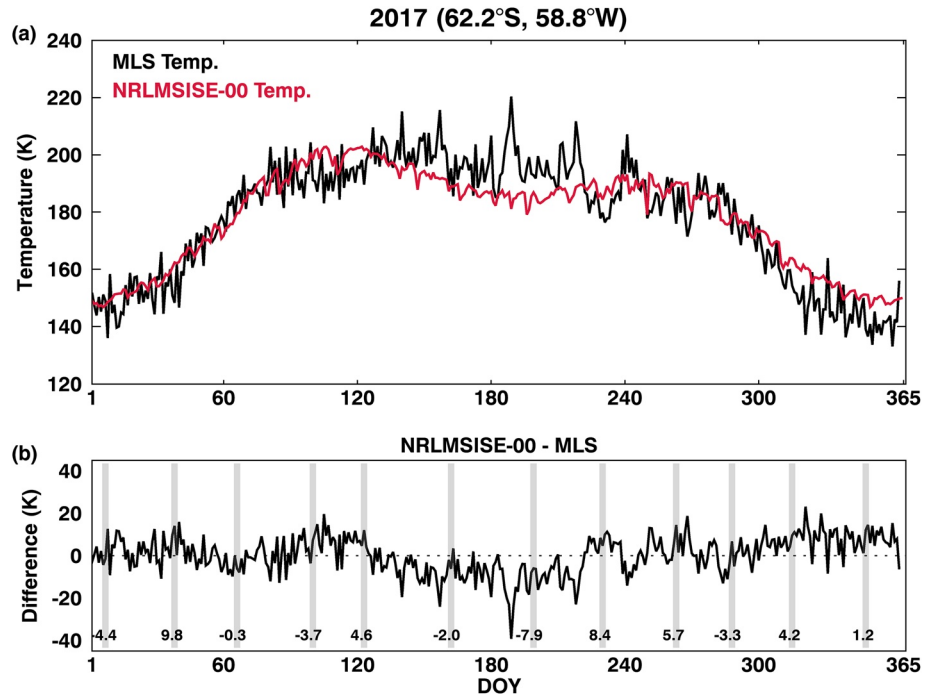


**Figure 7.** (a) Temperatures at 90 km from MLS (black line) and NRLMSISE-00 (red line) in 2017. (b) Difference between NRLMSISE-00 and MLS temperatures. Gray shaded areas indicate DOY 7, 38, 66, 100, 123, 157, 162, 199, 230, 263, 288, 315, and 348, which were selected for the meteor ablation model.

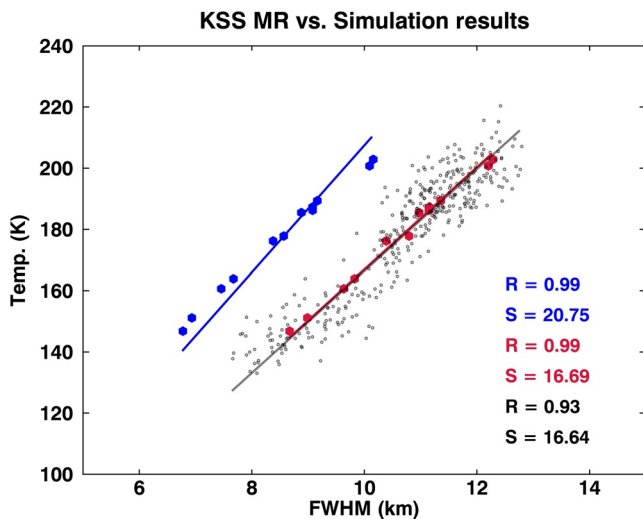


**Figure 8.** Daily full widths at half maximum of the meteor height distributions observed by the King Sejong Station meteor radar versus the Microwave Limb Sounder temperatures at 90 km (gray dots) and the full widths at half maximum of simulated meteor height distributions versus the temperatures at 90 km from NRLMSISE-00 (using the DOY 100/DOY 200 meteoroid group; red/blue dots) on specific days (DOY 7, 38, 66, 100, 123, 162, 199, 230, 263, 288, 315, and 348). The correlation coefficients (R)/slopes (S) are 0.92/16.64, 0.99/16.69, and 0.99/20.75 for observation and simulations, respectively. The solid lines indicate the regression lines.

with the peak and FWHM of  $10^{-6.2}$  and  $10^{1.3}$  kg, respectively. The variation of initial mass distribution should thus have little effect on the FWHM of the meteor height distribution.

In the simulation, we assumed that the height of maximized electron line density is the altitude of a meteor trail observed by the MR, which may not be so in the actual observation. However, this assumption can be statistically reasonable, given that the number of echoes is 17,123 and 13,072 for DOY 100 and 200, respectively. The assumption is also justified by the fact that the DOY 100 results match almost perfectly with the observed linear relation between the FWHM and temperature. The FWHM–temperature relation, however, would have been ruined due to the significant variation of the velocity distribution, as explained previously. We have confirmed that the high speed meteoroids are reduced in relatively cold season, mitigating the effect on the FWHM–temperature relation. Despite the uncertainties in the ablation model and the variation of meteoroid velocity distributions, the simulated results clearly explain that the mesospheric temperature variation is the main factor to determine the FWHM of the observed height distribution, which was the base for the FWHM method of temperature estimation by C. Lee et al. (2016).

## 5. Conclusion

We have developed a meteor ablation model that can calculate the meteoroid mass and electron line density of a meteor trail along the trajectory. By applying the ablation model to the meteor parameters observed by the KSS MR, we were able to obtain the daily initial mass and velocity distribution, which were used to simulate the meteor height distribution under various

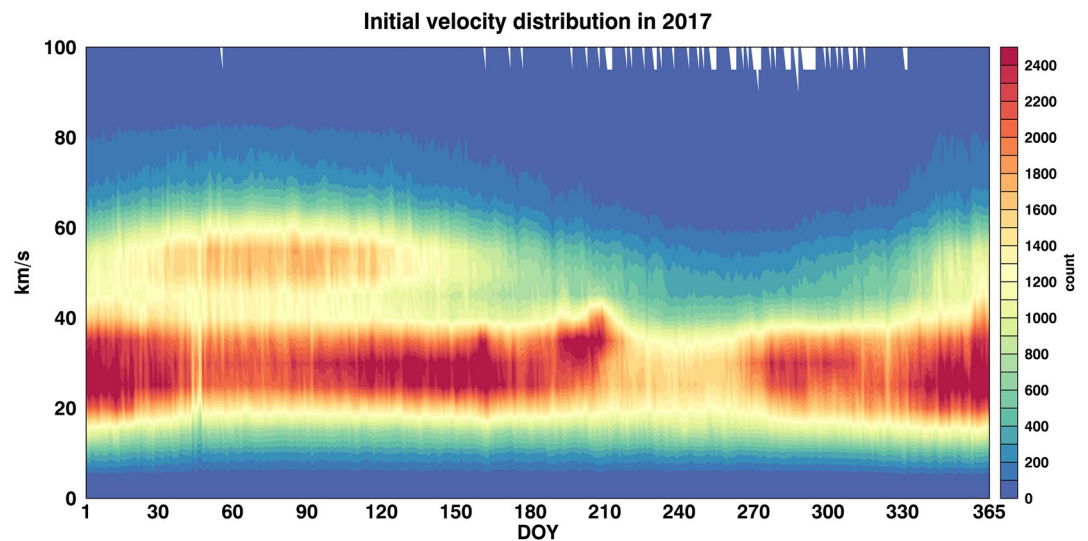


**Figure 9.** Annual variation of initial velocity distribution derived from King Sejong Station meteor radar in 2017.

atmospheric conditions. The simulation of meteor heights has clearly demonstrated that the meteor height distribution is dominantly dependent on the atmospheric condition, rather than on meteoroid characteristics. We found that the seasonal variation of meteoroid velocity distributions is significant but has only little effect on the variation of the meteor height distribution. We also found that the observed characteristics of meteoroids show a Gaussian distribution of logarithmic masses that has the average peak value of  $10^{-6.2}$  kg and this distribution is nearly invariable throughout the year. Thus, our study verifies the observed relation between the FWHM and

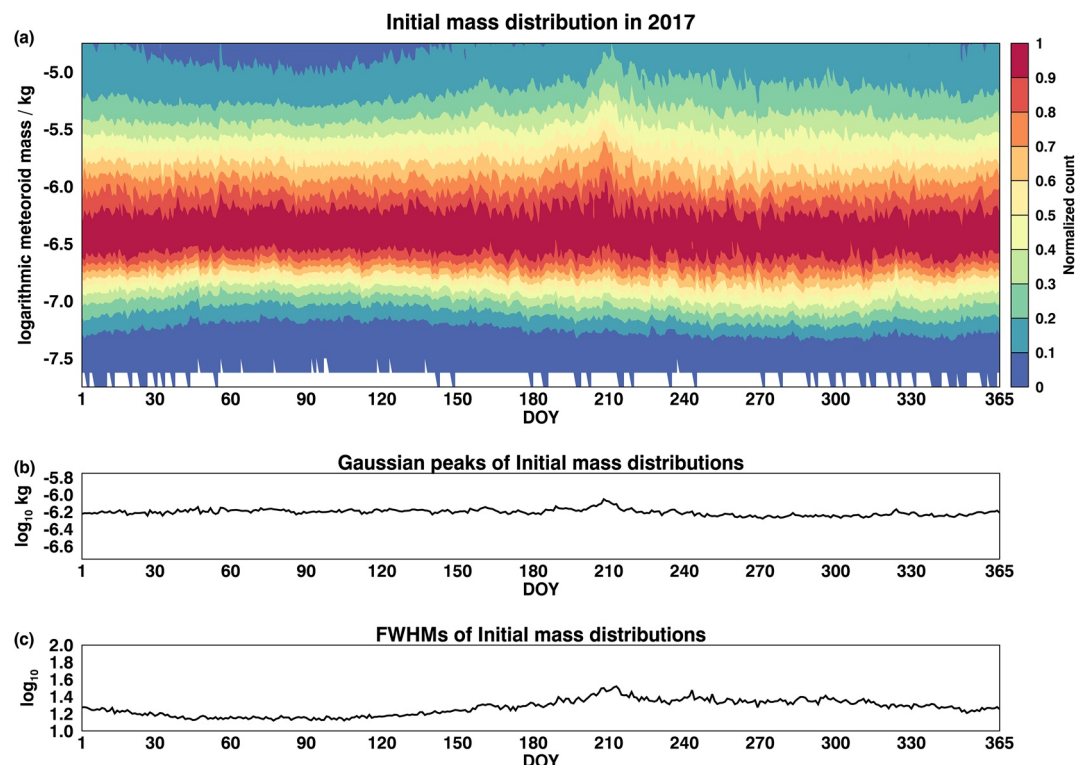


**Figure 10.** (a) Annual variation of initial mass distribution derived from King Sejong Station meteor radar. (b) Gaussian peaks of initial mass distributions. (c) Full widths at half maximum of initial mass distributions in 2017.

mesospheric temperature, which has been proposed as a new method of mesospheric temperature estimation from meteor height distributions measured by the MR (C. Lee et al., 2016).

## Data Availability Statement

The King Sejong Station meteor radar data are available at <https://dx.doi.org/doi:10.22663/KOPRI-KP-DC-00000806.1>. The Temperature and GPH data from Aura/MLS are available at <http://dx.doi.org/10.5067/Aura/MLS/DATA2021>. The NRLMSISE-00 data are available at <https://ccmc.gsfc.nasa.gov/modelweb/models/nrlmsise00.php>.

## Acknowledgments

This work was supported by the Korea Polar Research Institute (PE21020), Incheon, South Korea.

## References

- Baggaley, W. J. (2002). Radar observations. *Meteors in the Earth's Atmosphere*, 123–148.
- Brown, P., Stober, G., Schult, C., Krzeminski, Z., Cooke, W., & Chau, J. L. (2017). Simultaneous optical and meteor head echo measurements using the Middle Atmosphere Alomar Radar System (MAARSY): Data collection and preliminary analysis. *Planetary and Space Science*, 141, 25–34. <https://doi.org/10.1016/j.pss.2017.04.013>
- Campbell-Brown, M. D. (2008). Directional variation of sporadic meteor activity and velocity. *Earth, Moon, and Planets*, 102(1), 79–84. <https://doi.org/10.1007/s11038-007-9152-8>
- Campbell-Brown, M. D., & Koschny, D. (2004). Model of the ablation of faint meteors. *Astronomy & Astrophysics*, 418(2), 751–758. <https://doi.org/10.1051/0004-6361:20041001-1>
- Ceplecha, Z., Borovička, J., Elford, W. G., ReVelle, D. O., Hawkes, R. L., Porubčan, V., & Šimek, M. (1998). Meteor phenomena and bodies. *Space Science Reviews*, 84(3), 327–471. <https://doi.org/10.1023/A:1005069928850>
- Cervera, M. A., & Reid, I. M. (2000). Comparison of atmospheric parameters derived from meteor observations with CIRA. *Radio Science*, 35(3), 833–843. <https://doi.org/10.1029/1999RS002226>
- Chilson, P. B., Czechowsky, P., & Schmidt, G. (1996). A comparison of ambipolar diffusion coefficients in meteor trains using VHF radar and UV lidar. *Geophysical Research Letters*, 23(20), 2745–2748. <https://doi.org/10.1029/96GL02577>
- Close, S., Hamlin, T., Oppenheim, M., Cox, L., & Colestock, P. (2008). Dependence of radar signal strength on frequency and aspect angle of nonspecular meteor trails. *Journal of Geophysical Research*, 113(A6). <https://doi.org/10.1029/2007JA012647>
- Dyrland, M. E., Hall, C. M., Mulligan, F. J., Tsutsumi, M., & Sigernes, F. (2010). Improved estimates for neutral air temperatures at 90 km and 78°N using satellite and meteor radar data. *Radio Science*, 45(4). <https://doi.org/10.1029/2009RS004344>
- Dyrud, L., Wilson, D., Boerve, S., Trulsen, J., Pecseli, H., Close, S., et al. (2008). Plasma and electromagnetic wave simulations of meteors. *Advances in Space Research*, 42(1), 136–142. <https://doi.org/10.1016/j.asr.2007.03.048>
- Dyrud, L. P., Ray, L., Oppenheim, M., Close, S., & Denney, K. (2005). Modelling high-power large-aperture radar meteor trails. *Journal of Atmospheric and Solar-Terrestrial Physics*, 67(13), 1171–1177. <https://doi.org/10.1016/j.jastp.2005.06.016>
- Elford, W. G. (2004). Radar observations of meteor trails, and their interpretation using Fresnel holography: A new tool in meteor science. *Atmospheric Chemistry and Physics*, 4(4), 911–921. <https://doi.org/10.5194/acp-4-911-2004>
- Ellyett, C. D., & Kennewell, J. A. (1980). Radar meteor rates and atmospheric density changes. *Nature*, 287, 521–522. <https://doi.org/10.1038/287521a0>
- Eshleman, V. R. (1957). The theoretical length distribution of ionized meteor trails. *Journal of Atmospheric and Terrestrial Physics*, 10(2), 57–72. [https://doi.org/10.1016/0021-9169\(57\)90140-X](https://doi.org/10.1016/0021-9169(57)90140-X)
- Hall, C. M., Dyrland, M. E., Tsutsumi, M., & Mulligan, F. J. (2012). Temperature trends at 90 km over Svalbard, Norway (78°N 16°E), seen in one decade of meteor radar observations. *Journal of Geophysical Research*, 117(8). <https://doi.org/10.1029/2011JD017028>
- Hocking, W. K. (1999). Temperatures using radar-meteor decay times. *Geophysical Research Letters*, 26(21), 3297–3300. <https://doi.org/10.1029/1999GL003618>
- Hocking, W. K., Thayaparan, T., & Jones, J. (1997). Meteor decay times and their use in determining a diagnostic mesospheric temperature-pressure parameter: Methodology and one year of data. *Geophysical Research Letters*, 24(23), 2977–2980. <https://doi.org/10.1029/97GL03048>
- Holdsworth, D. A., Morris, R. J., Murphy, D. J., Reid, I. M., Burns, G. B., & French, W. J. R. (2006). Antarctic mesospheric temperature estimation using the Davis mesosphere-stratosphere-troposphere radar. *Journal of Geophysical Research*, 111(D5), 1–13. <https://doi.org/10.1029/2005JD006589>
- Holdsworth, D. A., Murphy, D. J., Reid, I. M., & Morris, R. J. (2008). Antarctic meteor observations using the Davis MST and meteor radars. *Advances in Space Research*, 42(1), 143–154. <https://doi.org/10.1016/j.asr.2007.02.037>
- Holdsworth, D. A., Reid, I. M., & Cervera, M. A. (2004). Buckland Park all-sky interferometric meteor radar. *Radio Science*, 39(5). <https://doi.org/10.1029/2003RS003014>
- Hunten, D. M., Turco, R. P., & Toon, O. B. (1980). Smoke and dust particles of meteoric origin in the mesosphere and stratosphere. *Journal of the Atmospheric Sciences*, 37(6), 1342–1357. [https://doi.org/10.1175/1520-0469\(1980\)037<1342:sadpom>2.0.co;2](https://doi.org/10.1175/1520-0469(1980)037<1342:sadpom>2.0.co;2)
- Jones, W. (1997). Theoretical and observational determinations of the ionization coefficient of meteors. *Monthly Notices of the Royal Astronomical Society*, 288(4), 995–1003. <https://doi.org/10.1093/mnras/288.4.995>
- Kaiser, T. R. (1954). Theory of the meteor height distribution obtained from radio-echo observations II. Sporadic meteors. *Monthly Notices of the Royal Astronomical Society*, 114(1), 52–62. <https://doi.org/10.1093/mnras/114.1.52>
- Kam, H., Kim, Y. H., Mitchell, N. J., Kim, J. H., & Lee, C. (2019). Evaluation of estimated mesospheric temperatures from 11-year meteor radar datasets of King Sejong Station (62°S, 59°W) and Esrange (68°N, 21°E). *Journal of Atmospheric and Solar-Terrestrial Physics*, 196, 105148. <https://doi.org/10.1016/j.jastp.2019.105148>
- Kim, J. H., Kim, Y. H., Jee, G., & Lee, C. (2012). Mesospheric temperature estimation from meteor decay times of weak and strong meteor trails. *Journal of Atmospheric and Solar-Terrestrial Physics*, 89(1), 18–26. <https://doi.org/10.1016/j.jastp.2012.07.003>
- Kim, J. H., Kim, Y. H., Lee, C. S., & Jee, G. (2010). Seasonal variation of meteor decay times observed at King Sejong Station (62.22°S, 58.78°W), Antarctica. *Journal of Atmospheric and Solar-Terrestrial Physics*, 72(11–12), 883–889. <https://doi.org/10.1016/j.jastp.2010.05.003>
- Lee, C., Jee, G., Kim, J. H., & Song, I. S. (2018). Meteor echo height ceiling effect and mesospheric temperature estimation from meteor radar observations. *Annales Geophysicae*, 36(5), 1267–1274. <https://doi.org/10.5194/angeo-36-1267-2018>

- Lee, C., Kim, J. H., Jee, G., Lee, W., Song, I. S. & Kim, Y. H. (2016). New method of estimating temperatures near the mesopause region using meteor radar observations. *Geophysical Research Letters*, 43(20), 580–585. <https://doi.org/10.1002/2016GL071082>
- Lee, C. S., Younger, J. P., Reid, I. M., Kim, Y. H., & Kim, J. H. (2013). The effect of recombination and attachment on meteor radar diffusion coefficient profiles. *Journal of Geophysical Research: Atmospheres*, 118(7), 3037–3043. <https://doi.org/10.1002/jgrd.50315>
- Lee, W., Song, I. S., Kim, J. H., Kim, Y. H., Jeong, S. H., Eswarajah, S., & Murphy, D. J. (2021). The observation and SD-WACCM simulation of planetary wave activity in the middle atmosphere during the 2019 southern hemispheric sudden stratospheric warming. *Journal of Geophysical Research: Space Physics*, 126, e2020JA029094. <https://doi.org/10.1029/2020JA029094>
- Lima, L. M., Batista, P. P., & Paulino, A. R. (2018). Meteor radar temperatures over the Brazilian low-latitude sectors. *Journal of Geophysical Research: Space Physics*, 123(9), 7755–7766. <https://doi.org/10.1029/2018JA025620>
- Lindblad, B. A. (1976). Meteor radar rates and the solar cycle. *Nature*, 259(5539), 99–101. <https://doi.org/10.1038/259099b0>
- Marshall, R. A., & Close, S. (2015). An FDTD model of scattering from meteor head plasma. *Journal of Geophysical Research: Space Physics*, 120(7), 5931–5942. <https://doi.org/10.1002/2015ja021238>
- Mathews, J. D., Janches, D., Meisel, D. D., & Zhou, Q. H. (2001). The micrometeoroid mass flux into the upper atmosphere: Arecibo results and a comparison with prior estimates. *Geophysical Research Letters*, 28(10), 1929–1932. <https://doi.org/10.1029/2000gl012621>
- McAuliffe, J. P., & Christou, A. A. (2006). Modelling meteor ablation in the Venusian atmosphere. *Icarus*, 180(1), 8–22. <https://doi.org/10.1016/j.icarus.2005.07.012>
- McKinley, D. W. R. (1961). *Meteor science and engineering*. McGraw-Hill.
- Meek, C. E., Manson, A. H., Hocking, W. K., & Drummond, J. R. (2013). Eureka, 80° N, SKiYMET meteor radar temperatures compared with Aura MLS values. *Annales Geophysicae*, 31(7), 1267–1277. <https://doi.org/10.5194/angeo-31-1267-2013>
- Moses, J. I. (1992). Meteoroid ablation in Neptune's atmosphere. *Icarus*, 99(2), 368–383. [https://doi.org/10.1016/0019-1035\(92\)90153-X](https://doi.org/10.1016/0019-1035(92)90153-X)
- Murad, E., & Williams, I. P. (2002). *Meteors in the Earth's atmosphere: Meteoroids and cosmic dust and their interactions with the Earth's upper atmosphere*. Cambridge University Press.
- Picone, J. M., Hedin, A. E., Drob, D. P., & Aikin, A. C. (2002). NRLMSISE-00 empirical model of the atmosphere: Statistical comparisons and scientific issues. *Journal of Geophysical Research*, 107(A12). <https://doi.org/10.1029/2002JA009430>
- Podolak, M., Pollack, J. B., & Reynolds, R. T. (1988). Interactions of planetesimals with protoplanetary atmospheres. *Icarus*, 73(1), 163–179. [https://doi.org/10.1016/0019-1035\(88\)90090-5](https://doi.org/10.1016/0019-1035(88)90090-5)
- Premkumar, B., Reddy, K. C., Yellaiah, G., & Kumar, K. K. (2019). Seasonal variations in vertical distribution of meteor decay time as observed from meteor radars at 8.5°N and 80°N. *Advances in Space Research*, 63(5), 1661–1669. <https://doi.org/10.1016/j.asr.2018.11.019>
- Rogers, L. A., Hill, K. A., & Hawkes, R. L. (2005). Mass loss due to sputtering and thermal processes in meteoroid ablation. *Planetary and Space Science*, 53(13), 1341–1354. <https://doi.org/10.1016/j.pss.2005.07.002>
- Singer, W., Bremer, J., Weiß, J., Hocking, W. K., Höffner, J., Donner, M., & Espy, P. (2004). Meteor radar observations at middle and Arctic latitudes Part 1: Mean temperatures. *Journal of Atmospheric and Solar-Terrestrial Physics*, 66(6–9), 607–616. <https://doi.org/10.1016/j.jastp.2004.01.012>
- Stober, G., Jacobi, C., Fröhlich, K., & Oberheide, J. (2008). Meteor radar temperatures over Collm (51.3°N, 13°E). *Advances in Space Research*, 42(7), 1253–1258. <https://doi.org/10.1016/j.asr.2007.10.018>
- Stober, G., Jacobi, C., & Singer, W. (2011). Meteoroid mass determination from underdense trails. *Journal of Atmospheric and Solar-Terrestrial Physics*, 73(9), 895–900. <https://doi.org/10.1016/j.jastp.2010.06.009>
- Taylor, A. D., & Elford, W. G. (1998). Meteoroid orbital element distributions at 1 AU deduced from the Harvard Radio Meteor Project observations. *Earth, Planets and Space*, 50(6–7), 569–575. <https://doi.org/10.1186/BF03352150>
- Vineeth, C., Pant, T. K., Antonita, M., Ramkumar, G., Devasia, C. V., & Sridharan, R. (2005). A comparative study of daytime mesopause temperatures obtained using unique ground based optical and meteor wind radar techniques over the magnetic equator. *Geophysical Research Letters*, 32(19). <https://doi.org/10.1029/2005GL023728>
- Yee, J., & Close, S. (2013). Plasma turbulence of nonspecular trail plasmas as measured by a high-power large-aperture radar. *Journal of Geophysical Research: Atmospheres*, 118(24), 13. <https://doi.org/10.1002/2013JD020247>
- Yi, W., Xue, X., Chen, J., Dou, X., Chen, T., & Li, N. (2016). Estimation of mesopause temperatures at low latitudes using the Kunming meteor radar. *Radio Science*, 51(3), 130–141. <https://doi.org/10.1002/2015RS005722>
- Younger, J. P. (2011). *Theory and applications of VHF meteor radar observations*. (PhD thesis). University of Adelaide.
- Younger, P. T., Astin, I., Sandford, D. J., & Mitchell, N. J. (2009). The sporadic radiant and distribution of meteors in the atmosphere as observed by VHF radar at Arctic, Antarctic and equatorial latitudes. *Annales Geophysicae*, 27(7), 2831–2841. <https://doi.org/10.5194/angeo-27-2831-2009>
- Zhou, Q. H., Morton, Y. T., Mathews, J. D., & Janches, D. (2004). Aspect sensitivity of VHF echoes from field aligned irregularities in meteor trails and thin ionization layers. *Atmospheric Chemistry and Physics*, 4(3), 685–692. <https://doi.org/10.5194/acp-4-685-2004>